

交变磁场辅助添加镍中间层镁/钢激光熔钎焊接头的组织性能研究

戎易, 程东海*, 熊震宇, 陈益平, 刘钊泽

南昌航空大学航空制造工程学院, 江西 南昌 330063

摘要 采用激光熔钎焊技术进行镁/钢异种材料的搭接试验,通过添加镍中间层调控焊缝成分,并通过外加纵向交变磁场调控接头的组织形貌,从而提升接头的力学性能。试验结果表明:强烈的电磁搅拌促进了镁、镍、铁元素之间的扩散与反应;外加交变磁场后,镁侧焊缝熔池中的带状 Fe-Ni 固溶体使接头的机械咬合作用增强,金属间化合物层的类熔焊区与类钎焊区未生成树枝状 AlNi,类熔焊区形成的连续的纳米级 AlNi 层对接头具有强化作用,提高了接头的力学性能。接头的拉剪强度随着励磁电流 I_E 与励磁频率 f 的增加呈先增大后减小的趋势,当激光功率 $P=1250\text{ W}$,焊接速度 $v=20\text{ mm/s}$, $I_E=1.2\text{ A}$, $f=35\text{ Hz}$ 时,接头的拉剪强度最高,达到了 228 MPa,比无交变磁场时提高了约 15%。

关键词 激光技术; 激光熔钎焊; 交变磁场; 机械咬合; 金属间化合物层; 拉剪强度

中图分类号 TG442

文献标志码 A

doi: 10.3788/CJL202148.2202005

1 引言

异种材料焊接的复合结构不仅可以节省材料,还能发挥各自的性能优势^[1-2]。镁/钢异种材料的连接能实现结构轻量化设计与节能减排,在航空、船舶、汽车等领域具有很高的应用价值^[3]。然而,实现镁/钢异种材料的高质量连接存在以下问题:1)镁合金和钢的熔、沸点差异较大,两者的同时熔化极其困难;2)镁和钢的晶格类型不同;3)镁合金与钢的热物理性能差异较大,这会导致焊后产生较大的残余应力;4)根据镁-钢的二元相图,它们在液态下极难互溶,导致焊后接头极易分层脱离^[4]。

为解决镁/钢之间不互溶也不生成金属间化合物的问题,研究人员通过外加镍、铜、银、锌、锡、Cu-Zn 和 Zn-xAl 中间层或镀层等措施来促进界面化合物的生成^[5-12],使焊接接头获得了较高的力学性能。然而,通过外加合金这一措施也不能使接头界面处得到理想厚度的金属间化合物层。

在激光焊接过程中施加交变磁场,磁场与感应电流作用产生电磁力,交变电磁力可促使熔池产生

正反两个方向的旋转运动,加剧熔池中的对流运动^[13]。Avilov 等^[14]对 2205 双相钢板进行了激光全熔透对接试验,他们采用一种非接触式交流感应电磁系统来防止焊根下垂,提高了焊接质量。刘洪喜等^[15]在激光熔覆过程中施加交变磁场后发现:熔池金属液表面产生了趋肤效应和交变电磁力,电磁力促使熔覆层顶部组织由树枝晶向等轴晶转变;熔池内液态金属的对流加剧,改善了熔覆层中的裂纹、气孔等缺陷。丁浩等^[16]在 DC51D+AZ 镀锌钢与 6061 铝合金激光对接焊试验中施加了交变磁场,结果发现,磁场的搅拌作用能改善焊缝形貌,减少焊缝中的气孔缺陷,细化针状 FeAl₃ 相,抑制脆性 Fe/Al 化合物的生长,接头的力学性能得到有效提高。所查资料显示,交流磁场辅助同种或异种材料的激光焊接已有人进行了一定程度的研究,外加交流磁场主要改变熔池运动,从而调控接头界面层的化合物,提高接头的力学性能。

综上所述,外加交变磁场能加剧熔池运动,促进元素之间的扩散与反应,改善添加镍中间层的镁/钢异种材料熔钎焊接头中金属间化合物的形貌与分

收稿日期: 2021-03-24; 修回日期: 2021-05-11; 录用日期: 2021-06-25

基金项目: 国家自然科学基金(51965045)

通信作者: *70269@nchu.edu.cn

布,从而提高接头的力学性能。镍在凝固时能够与镁、铝、铁元素分别形成金属间化合物和固溶体。鉴于此,本研究团队在镁合金和钢中间添加镍片,进行了交变磁场辅助镁/钢异种金属的激光熔钎焊接试验,对比研究了有无外加交变磁场下接头中的元素分布以及接头的微观组织和力学性能,为通过外加交变磁场进一步改善添加镍中间层的镁/钢异种金属连接技术提供相关数据支撑。

2 试验方法

本次试验中的母材选用尺寸为 $120\text{ mm} \times 60\text{ mm} \times 1\text{ mm}$ 的 AZ31B 镁合金 (Mg-3Al-1Zn-0.2Mn-0.1Si) 和 Q235 低碳钢 (Fe-0.7Mn-0.3Si-0.2C), 中间层是尺寸为 $60\text{ mm} \times 10\text{ mm} \times 0.1\text{ mm}$ 的 N6 镍片。焊接试验采用的主要设备是 IPG 公司的 YLS-6000CUT 型光纤激光器, 其发射激光的波长为 $1.07\text{ }\mu\text{m}$ 。焊接时, 试样的上表面采用纯度为 99% 的氩气进行保护, 氩气以 15 L/min 的流速从直径为 16 mm 的喷嘴中喷出。将 AZ31B 镁合金置于 Q235 低碳钢之上, 并在两者之间添加 0.1 mm 厚的镍片, 然后用夹具将其固定。在外加交变磁场下对添加镍中间层的镁/钢进行搭接焊的示意图如图 1 所示。焊接结束后, 采用线切割机沿垂直于焊缝方向进行切割, 制取试样, 然后采用 XQ-1 型热镶嵌机将试样制作成镶嵌块, 对其进行打磨、抛光等处理。经过前期的预试验, 选定的最佳焊接工艺参数为: 激光功率 $P=1250\text{ W}$, 焊接速度 $v=20\text{ mm/s}$; 选定的交流磁场参数为: 励磁电流 $I_E=0.8\sim 2.0\text{ A}$ (每 0.2 A 为一个递增单位), 励磁频率 $f=15\sim 55\text{ Hz}$ (每 10 Hz 为一个递增单位)。采用光学显微镜 (OM)、扫描电子显微镜 (SEM) 和能谱仪 (EDS)

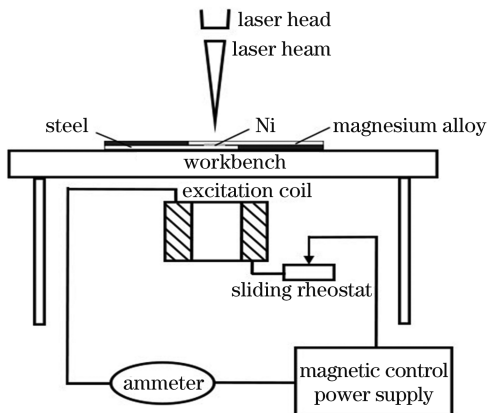


图 1 外加交变磁场焊接装置示意图

Fig. 1 Schematic of welding device with alternating magnetic field

研究外加纵向交变磁场对镁侧焊缝、钢侧焊缝、界面金属间化合物层 (IMC 层) 的影响; 使用 WDW-100 型电子万能拉伸试验机对接头进行拉剪测试, 拉伸速度为 0.5 mm/min 。拉剪试样的尺寸如图 2 所示, 每组参数下拉伸 3 组试样, 将得到的 3 组参数求平均值, 计算对应的拉剪强度。

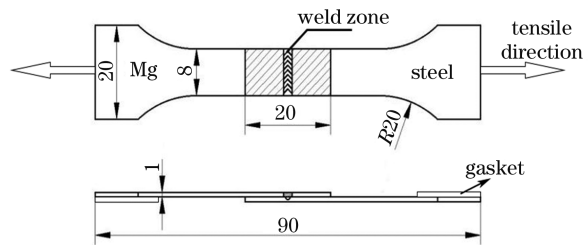


图 2 拉剪试样的尺寸

Fig. 2 Size of tensile and shear specimen

3 分析与讨论

3.1 接头区域的元素分布

图 3、4 分别是未施加交变磁场以及施加交变磁场情况下得到的接头区域的焊缝形貌及元素分布情况。由图 3(a)、图 4(a) 所示的接头区域的焊缝形貌可以发现, 接头焊缝由镁侧焊缝、IMC 层、钢侧焊缝组成。在未施加交变磁场的情况下, 镁侧焊缝有少量类球状钢颗粒; 外加交变磁场后, 镁侧焊缝中的类球状钢颗粒增多。对比图 3(b) 和图 4(b) 可以发现, 镁元素主要集中在镁侧焊缝内, 且外加交变磁场后镁元素在钢侧的分布更广, 说明镁元素向钢侧发生了明显的扩散。对比图 3(c) 和图 4(c) 可以发现, 铁元素分布在钢侧焊缝、钢母材和镁侧焊缝中, 且外加交变磁场后铁元素在镁侧焊缝中分布得更多, 说明铁元素向镁侧的扩散更为明显。这是因为在交变磁场的作用下, 微量熔化的钢扩散到了镁侧焊缝中。对比图 3(d) 和图 4(d) 可以发现, 镍元素主要分布在钢侧焊缝, 且外加交变磁场后镍元素的分布范围扩大。这是由于熔池内部的电磁力驱动混杂着熔融镍的金属液体流动, 使镍元素扩散得更加充分。由图 3(e) 和图 4(e) 可以发现铝元素扩散至整个界面。对比图 3(f) 和图 4(f) 可以发现, 未施加交变磁场时氧元素集中在镁元素与铁元素的过渡区域, 外加交变磁场后, 熔池内基本没有氧元素分布, 唯一较为集中的氧元素分布区域是左侧镍片与钢之间的间隙。

综上所述, 外加交变磁场后, 强烈的电磁搅拌促进了镁、镍、铁元素三者之间的扩散与反应, 使原本难以连接的镁合金与钢通过镍的桥梁作用调控焊缝

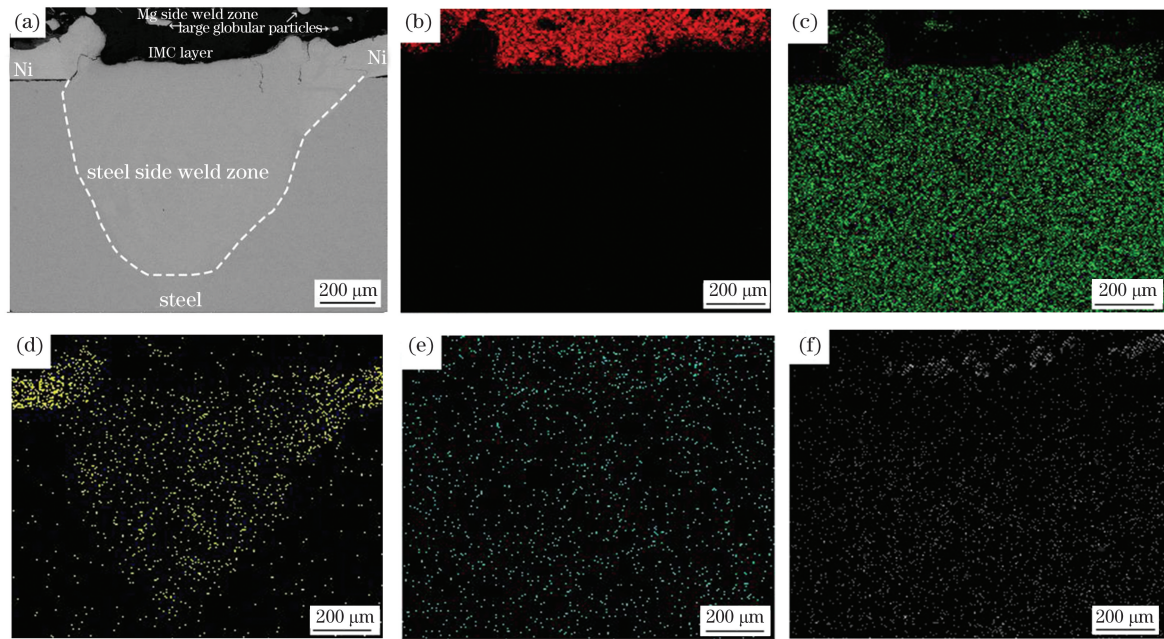


图 3 未施加交变磁场时接头区域的元素分布。(a) 焊缝区域的整体形貌；(b) 镁元素分布；(c) 铁元素分布；(d) 镍元素分布；(e) 铝元素分布；(f) 氧元素分布

Fig. 3 Element distribution of welded joint without alternating magnetic field. (a) Overall morphology of weld zone; (b) Mg element distribution; (c) Fe element distribution; (d) Ni element distribution; (e) Al element distribution; (f) O element distribution

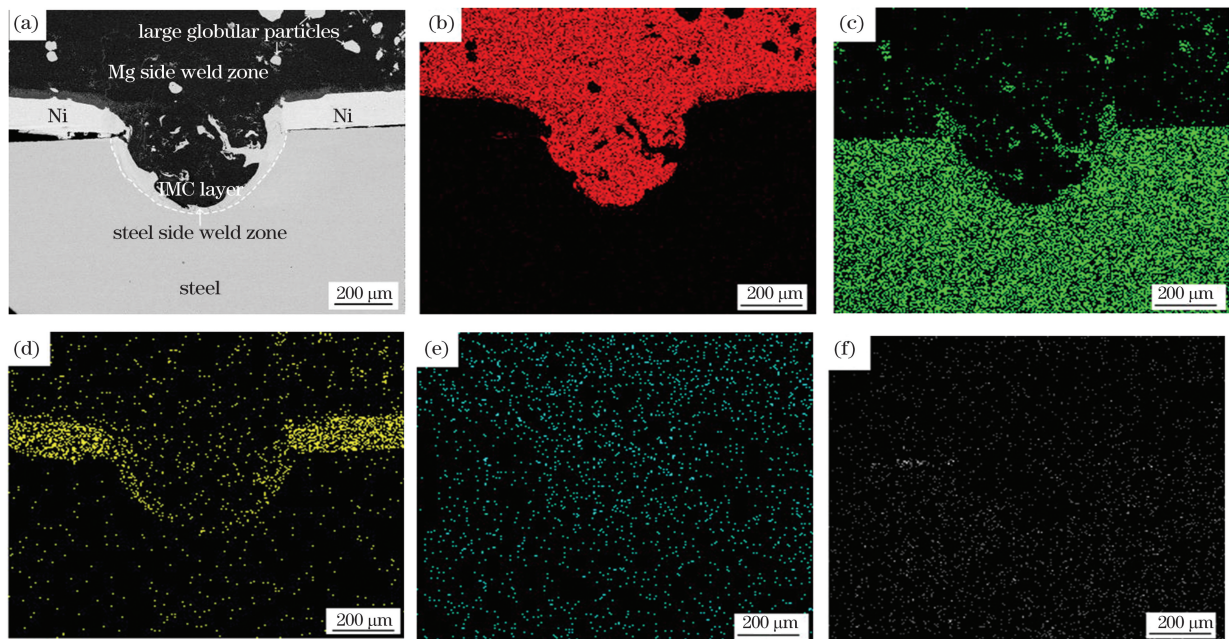


图 4 外加交变磁场下接头区域的元素分布。(a) 焊缝区域的整体形貌；(b) 镁元素分布；(c) 铁元素分布；(d) 镍元素分布；(e) 铝元素分布；(f) 氧元素分布

Fig. 4 Element distribution of welded joint with alternating magnetic field. (a) Overall morphology of weld zone; (b) Mg element distribution; (c) Fe element distribution; (d) Ni element distribution; (e) Al element distribution; (f) O element distribution

成分,实现更好的冶金结合。为进一步研究有无外加交变磁场情况下接头的微观组织,采用 SEM、EDS 研究了熔钎焊接头的组织结构。

3.2 微观组织分析

图 5 和图 6 分别为未施加交变磁场和施加交变磁场下接头不同区域的 SEM 图像,其中,图 5(b)~

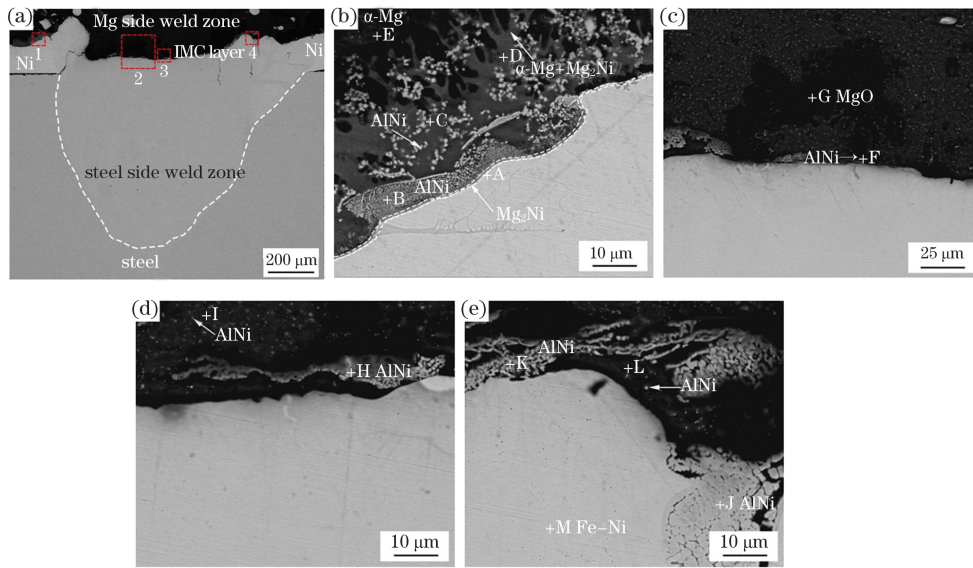


图 5 未施加交变磁场时接头不同位置处的 SEM 图像。(a) 接头横截面；(b) 1 区的放大图；(c) 2 区的放大图；(d) 3 区的放大图；(e) 4 区的放大图

Fig. 5 SEM images at different positions of welded joint without alternating magnetic field. (a) Cross-section of welded joint; (b) amplified image of region 1; (c) amplified image of region 2; (d) amplified image of region 3; (e) amplified image of region 4

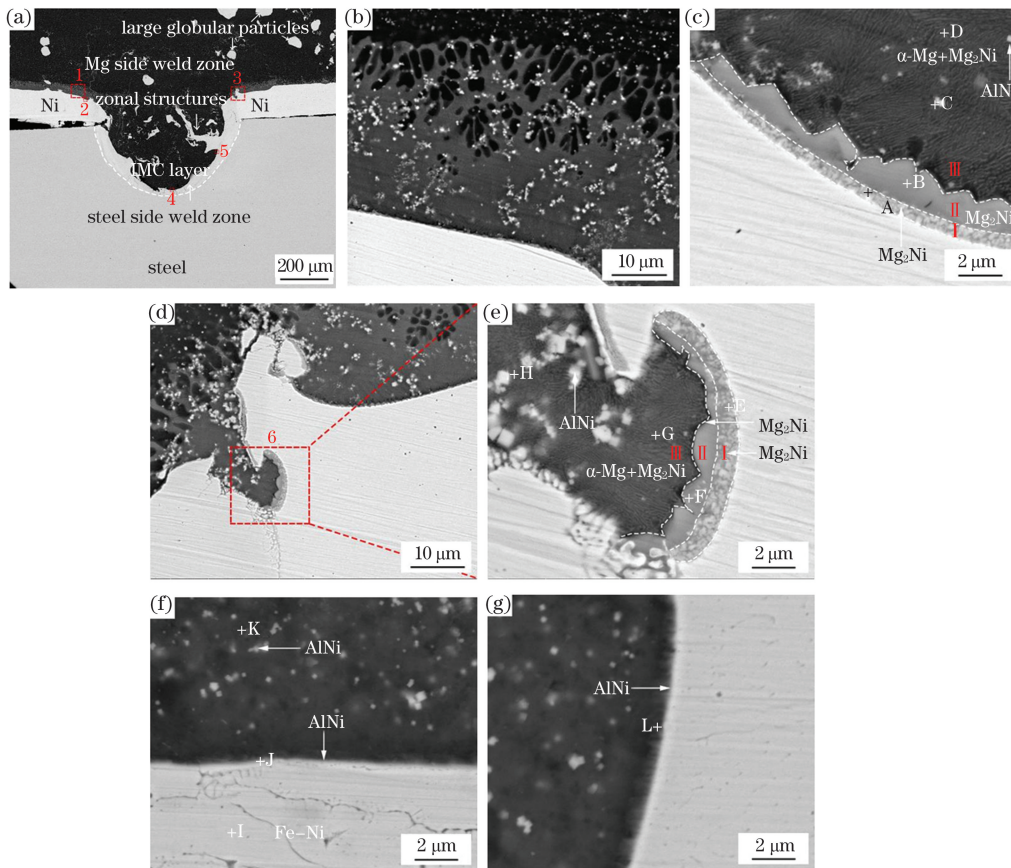


图 6 外加交变磁场下接头不同位置处的 SEM 图像。(a) 横截面；(b) 1 区的放大图；(c) 2 区的放大图；(d) 3 区的放大图；(e) 6 区的放大图；(f) 4 区的放大图；(g) 5 区的放大图

Fig. 6 SEM images at different positions of welded joint with alternating magnetic field. (a) Cross-section; (b) amplified image of region 1; (c) amplified image of region 2; (d) amplified image of region 3; (e) amplified image of region 6; (f) amplified image of region 4; (g) amplified image of region 5

(e)分别为图 5(a)中 1、2、3、4 区域的放大图,图 6(b)~(g)分别为图 6(a)、(d)中 1、2、3、6、4、5 区域的放大图。观察可知,接头上存在微裂纹,这些裂纹主要由热应力产生。结合图 5(a)、(d)、(e)和图 6(a)、(f)、(g)所示的 SEM 图像以及表 1 所示的图 5 中 I 点和 M 点的能谱结果、表 2 所示的图 6 中的 K 点和 I 点的能谱结果可以发现,无论有无外加交变磁场,镁侧焊缝都由 α -Mg 和 AlNi 组成,钢侧

焊缝均由 Fe-Ni 固溶体组成。外加交变磁场后,镁侧焊缝熔池中出现了带状 Fe-Ni 固溶体组织,该组织能增加界面层与焊缝之间的结合面积,使接头的机械咬合作用增强。这是由于外加交变磁场后,熔池金属表面的趋肤效应与交变电磁力对熔池中的液态金属进行了更为剧烈的搅拌,铁与镍元素向镁侧焊缝扩散得更明显,导致熔池内部存在带状 Fe-Ni 组织。

表 1 未施加交变磁场时镁/钢接头不同位置处的 EDS 分析

Table 1 EDS analysis of Mg/steel welded joint at different positions when alternating magnetic field is not applied

| Element | Atomic fraction /% | | | | | | |
|----------------|--------------------|-------|-------|---------------------------------|--------------|-------|-------|
| | A | B | C | D | E | F | G |
| Mg | 75.62 | 72.68 | 68.86 | 88.41 | 83.48 | 43.44 | 39.74 |
| Al | 1.23 | 13.43 | 13.70 | - | 16.52 | 27.04 | 0.93 |
| Fe | 11.86 | 1.22 | 0.78 | 0.64 | - | 5.68 | 0.49 |
| Ni | 11.29 | 12.68 | 16.66 | 10.95 | - | 23.84 | - |
| O | - | - | - | - | - | - | 58.85 |
| Possible phase | Mg ₂ Ni | AlNi | AlNi | α -Mg+Mg ₂ Ni | α -Mg | AlNi | MgO |

| Element | Atomic fraction /% | | | | | |
|----------------|--------------------|-------|-------|-------|-------|-------|
| | H | I | J | K | L | M |
| Mg | 34.95 | 96.96 | 41.56 | 45.97 | 46.33 | - |
| Al | 34.74 | 2.25 | 26.82 | 21.42 | 25.06 | - |
| Fe | 4.47 | - | 3.64 | 4.77 | 3.08 | 80.35 |
| Ni | 25.84 | 0.79 | 27.98 | 27.84 | 25.53 | 19.65 |
| O | - | - | - | - | - | - |
| Possible phase | AlNi | AlNi | AlNi | AlNi | AlNi | Fe-Ni |

表 2 外加交变磁场时镁/钢接头不同位置处的 EDS 分析

Table 2 EDS analysis of Mg/steel welded joint at different positions when alternating magnetic field is applied

| Element | Atomic fraction /% | | | | | |
|----------------|--------------------|--------------------|-------|---------------------------------|--------------------|--------------------|
| | A | B | C | D | E | F |
| Mg | 54.11 | 70.97 | 73.04 | 90.21 | 54.11 | 70.85 |
| Al | 1.77 | 0.59 | 9.47 | 0.00 | 1.77 | 0.38 |
| Fe | 0.37 | 0.57 | 1.52 | 0.00 | 0.37 | 0.72 |
| Ni | 43.75 | 27.87 | 15.97 | 9.79 | 43.75 | 28.05 |
| Possible phase | Mg ₂ Ni | Mg ₂ Ni | AlNi | α -Mg+Mg ₂ Ni | Mg ₂ Ni | Mg ₂ Ni |

| Element | Atomic fraction /% | | | | | |
|----------------|---------------------------------|-------|-------|-------|-------|-------|
| | G | H | I | J | K | L |
| Mg | 88.61 | 38.68 | 1.65 | 66.61 | 82.36 | 72.40 |
| Al | 0.00 | 24.80 | 1.27 | 7.91 | 8.82 | 3.19 |
| Fe | 0.52 | 8.44 | 75.04 | 15.14 | 0.91 | 15.57 |
| Ni | 10.87 | 28.08 | 22.04 | 10.34 | 7.91 | 8.84 |
| Possible phase | α -Mg+Mg ₂ Ni | AlNi | Fe-Ni | AlNi | AlNi | AlNi |

无论有无外加交变磁场,接头中的镍片都没有完全熔化,两侧未完全熔化的镍与镁、铝反应,形成类似钎焊的区域。中间熔化的镍与镁、铝反应后与铁固溶,形成类似熔焊的区域。图 5(a)IMC 层中的

1 区发生的反应类似于钎焊,2 区、3 区、4 区发生的反应类似于熔焊。同理,图 6(a)IMC 层中的 1 区、2 区、3 区、6 区发生的反应类似于钎焊,4 区、5 区的反应类似于熔焊。图 5(b)是图 5(a)中 1 区的放大图,

可以发现:没有施加交变磁场时,接头两侧的钎焊区存在 IMC 层,该层可以分为 3 层,分别是层状 Mg_2Ni (I 层)、树枝状 $AlNi$ (II 层)、(α -Mg + Mg_2Ni) 共晶组织及弥散分布的白色方形颗粒状 $AlNi$ (III 层);在熔焊区域的 IMC 层存在树枝状 $AlNi$ 相。观察图 6(b)~(c) 所示的图 6(a) 中 1 区、2 区、3 区、6 区的放大图可以发现:外加交变磁场后,两侧钎焊区的 IMC 层也可以分成 3 层,分别是颗粒状 Mg_2Ni (I 层)、锯齿状 Mg_2Ni (II 层)、(α -Mg + Mg_2Ni) 共晶组织及白色方形颗粒状 $AlNi$ (III 层);熔焊区域的树枝状 $AlNi$ 消失,但存在一层纳米级层状 $AlNi$ 相。

综上所述,无论有无外加磁场,IMC 层都由 Mg_2Ni 、 $AlNi$ 和 (α -Mg + Mg_2Ni) 共晶组织组成,但外加交变磁场后两侧钎焊区与熔焊区 IMC 层化合物的形貌与分布发生了变化,具体表现在:类钎焊区与熔焊区 IMC 层中的树枝状 $AlNi$ 相消失,类钎焊区 Mg_2Ni 的形态由层状变为锯齿状,熔焊区 IMC 层中出现连续的纳米级 $AlNi$ 层。外加交变磁场后,钎焊区 IMC 层中的 Mg_2Ni 由层状转变为锯齿状,机械咬合作用增强;同时,锯齿状 Mg_2Ni 增加了其与 (α -Mg + Mg_2Ni) 共晶组织的接触面积,有利于提高力学性能。熔焊区出现的连续纳米级 $AlNi$ 层对熔钎焊接头具有强化作用^[17],使接头的力学性能提高。对接头的剪切强度进行测试后发现:不施加交变磁场时,接头的最高拉剪强度为 198 MPa;外加交变磁场 ($I_E = 1.2$ A, $f = 35$ Hz) 后,接头的最高拉剪强度达到 228 MPa,比不施加交变磁场时提高了约 15%。这是由于外加交变磁场改变了熔池的温

度梯度,易生成较多的 Mg_2Ni 化合物。在磁场的搅拌作用下,IMC 层呈锯齿状。在类熔焊区域,一部分镍元素与铁元素形成液态的铁镍混合物,当 Fe-Ni 温度降至凝固点附近时,就会形成 Fe-Ni 固溶体,而 $AlNi$ 化合物的熔点明显高于 Fe-Ni 固溶体的熔点^[18],因此,在 Fe-Ni 固溶体凝固前,部分镍原子会与镁合金溶池中的铝发生反应,优先形成 $AlNi$ 化合物。在交变磁场的作用下,镍原子扩散的范围更广,类熔焊区未生成树枝状 $AlNi$,而是生成了一层连续的纳米级 $AlNi$ 层。另外,对比图 5(c) 与图 6(f) 可以发现外加磁场后接头中的氧化物减少了。

3.3 力学性能分析

图 7(a) 为添加镍中间层的镁/钢激光熔钎焊搭接接头拉剪断裂后的形貌,接头在拉剪断裂后基本无变形。将接头拉剪断裂时的强度定义为拉剪强度 σ_b ,其计算公式为

$$\sigma_b = \frac{F}{S}, \quad (1)$$

$$S = d \cdot h, \quad (2)$$

式中: σ_b 为拉剪强度,MPa; F 为拉剪力; S 为实际连接面积, mm^2 ; d 为接头实际连接的宽度,mm; h 为拉伸试样的宽度,mm。接头实际连接的宽度 d 如图 7(b) 标注所示。通过 OM 与 SEM 观察拉剪断裂后的试样可以发现未熔化的镍片还残留在镁侧。由于钢与镍片之间存在间隙,试样沿着钢与镍片之间的间隙与类熔焊区 IMC 层断裂,所以实际的宽度 d 如图 7(b) 所示,不计算接头伪连接区域。采用 CAD 软件测量实际宽度,再进行拉剪强度的计算。

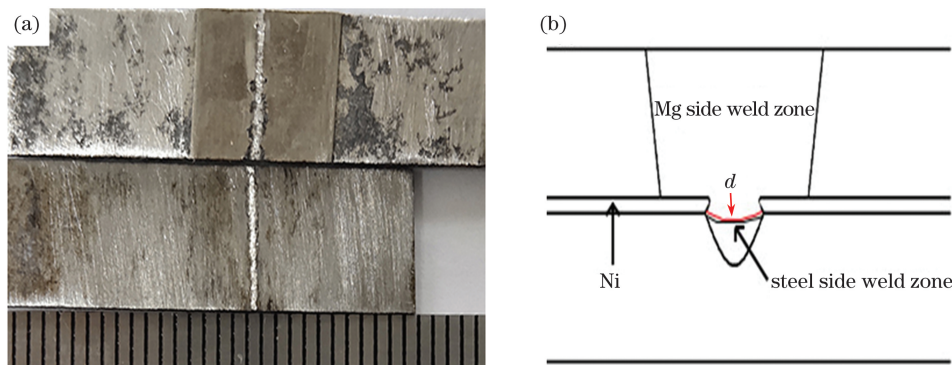


图 7 拉剪断裂后的接头试样及示意图。(a) 拉剪断裂后的激光熔钎焊搭接接头试样;(b) 接头实际连接的宽度

Fig. 7 Welded joint sample and schematic diagram after tensile and shear fracture. (a) Welded joint of laser brazing lap joint after tensile and shear fracture; (b) actual width of the connection

当 $P = 1250$ W, $v = 20$ mm/s 时,未施加交变磁场的接头的最高拉剪强度可达到 198 MPa。保持焊接工艺参数不变,在激光焊接过程中外加交变磁场。

图 8(a)、(b) 是励磁电流 I_E 与励磁频率 f 对接头拉剪强度的影响,可以看出,随着励磁电流 I_E 与励磁频率 f 增大,接头的拉剪强度均呈现出先上升后下

降的趋势。当励磁电流 $I_E=0.8\text{ A}$ 时,由于励磁电流过小,熔池中受到的电磁力较小,交变磁场对界面化合物的调控作用不明显,拉剪强度提升得不明显;随着励磁电流继续增大至 1.6 A ,熔池中的电磁搅拌作用过强,熔池中的温度梯度变化大,导致热应力大,产生了较多裂纹,接头的拉剪强度降低。在励磁电流 $I_E=1.2\text{ A}$ 的情况下,当励磁频率 $f=15\text{ Hz}$ 时,过低的频率作用在熔池中,对熔池的搅拌能力较弱;随着励磁频率增大,接头的拉剪强度增大;当励磁频率增大至 55 Hz 时,接头的拉剪强度总体上大于无磁场时接头的拉剪强度。这是由于过快的频

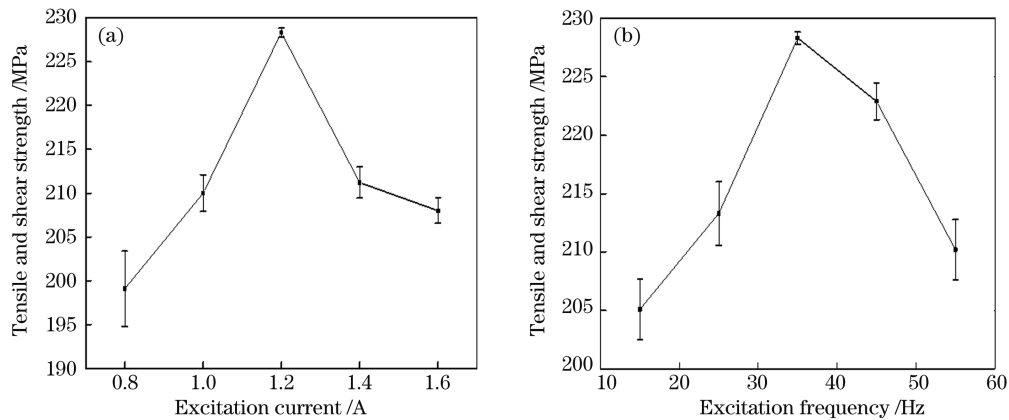


图 8 励磁电流和励磁频率对接头拉剪强度的影响。(a)励磁电流的影响;(b)励磁频率的影响

Fig. 8 Effects of excitation current and frequency on tensile and shear strength of welded joint. (a) Influence of excitation current; (b) influence of excitation frequency

4 结 论

通过外加交变磁场来调控添加镍中间层的镁/钢接头中化合物的分布,实现了提高接头力学性能的目的。外加交变磁场后,强烈的电磁搅拌促进了焊缝中镁、镍、铁元素之间的扩散与反应。

接头镁侧焊缝熔池中的带状 Fe-Ni 固溶体与 IMC 层类钎焊区呈锯齿状的 Mg_2Ni 使机械咬合作用增强,IMC 层类熔焊区中连续的纳米级 AlNi 层对熔钎焊接头具有强化作用,提高了接头的性能。添加交变磁场后,接头的拉剪强度均比无磁场时高,而且接头的拉剪强度随着励磁电流、励磁频率的增大呈先增大后减小的趋势。当 $P=1250\text{ W}$, $v=20\text{ mm/s}$, $I_E=1.2\text{ A}$, $f=35\text{ Hz}$ 时,接头的拉剪强度最高,可达到 228 MPa ,比无磁场时提高了约 15% 。

参 考 文 献

[1] Chen B Q, Xiong H P, Sun B B, et al. Microstructures and properties of laser welded

率使得磁场在熔池中的分布受到扰乱,熔池中心受到的电磁搅拌作用减弱。当 $P=1250\text{ W}$, $v=20\text{ mm/s}$, $I_E=1.2\text{ A}$, $f=35\text{ Hz}$ 时,拉剪强度达到最大值 228 MPa ,比无外加交变磁场时提高了约 15% 。这是由于外加交变磁场对界面化合物进行了调控,镁侧焊缝熔池中带状 Fe-Ni 固溶体与钎焊区 IMC 层中锯齿状 Mg_2Ni 的机械咬合作用增强,同时,熔焊区出现了连续的纳米级 AlNi 层。镍中间层的加入使接头实现了冶金结合,同时,外加交变磁场调控了界面化合物的形貌,使接头的力学性能提高。

dissimilar $\text{Ti}_3\text{Al}/\text{GH4169}$ joints[J]. Chinese Journal of Lasers, 2018, 45(4): 0402004.

陈冰清,熊华平,孙兵兵,等. $\text{Ti}_3\text{Al}/\text{GH4169}$ 异种材料激光焊接头的组织及性能[J]. 中国激光, 2018, 45(4): 0402004.

[2] Wu X, Zhang P L, Tang M, et al. Formation and microstructure characteristics in spot welding of dissimilar Cu-Al foil by nanosecond laser scanning [J]. Chinese Journal of Lasers, 2019, 46(4): 0402006.

吴希,张培磊,唐满,等. 铜-铝异种箔片纳秒激光扫描点焊成形及组织特征[J]. 中国激光, 2019, 46(4): 0402006.

[3] Casalino G, Guglielmi P, Lorusso V D, et al. Laser offset welding of AZ31B magnesium alloy to 316 stainless steel [J]. Journal of Materials Processing Technology, 2017, 242: 49-59.

[4] Rong Y, Hu D A, Cheng D H, et al. Research status of fusion welding of magnesium alloy and steel dissimilar materials [J]. Transactions of Materials and Heat Treatment, 2021, 42(1): 24-33.

戎易,胡德安,程东海,等. 镁合金-钢异种材料熔化焊研究现状[J]. 材料热处理学报, 2021, 42(1): 24-

- 33.
- [5] Zhou D W, Liu J S, Tan Z, et al. Effects of Sn-foil addition on the microstructure and mechanical properties of laser welding joint for dual phase steel and magnesium alloy [J]. *SN Applied Sciences*, 2019, 1(7): 1-12.
- [6] Tan C W, Xiao L Y, Liu F Y, et al. Influence of laser power on the microstructure and mechanical properties of a laser welded-brazed Mg alloy/Ni-coated steel dissimilar joint [J]. *Journal of Materials Engineering and Performance*, 2017, 26(6): 2983-2997.
- [7] Koba M, Araki T, Nambu S, et al. Bonding interface formation between Mg alloy and steel by liquid-phase bonding using the Ag interlayer [J]. *Metallurgical and Materials Transactions A*, 2012, 43(2): 592-597.
- [8] Miao Y G, Wu B T, Xu X F, et al. Effect of heat input on microstructure and mechanical properties of joints made by bypass-current MIG welding-brazing of magnesium alloy to galvanized steel [J]. *Acta Metallurgica Sinica (English Letters)*, 2014, 27(6): 1038-1045.
- [9] Liu L M, Qi X D. Strengthening effect of nickel and copper interlayers on hybrid laser-TIG welded joints between magnesium alloy and mild steel [J]. *Materials & Design*, 2010, 31(8): 3960-3963.
- [10] Song G, Wang J, Yu J W, et al. Study on fusion welding of magnesium alloy to steel by hybrid laser-TIG welding with interlayer [J]. *Transactions of the China Welding Institution*, 2016, 37(5): 69-72, 132. 宋刚, 王杰, 于景威, 等. 添加过渡层的镁合金/钢激光-TIG 电弧复合熔化焊接机制 [J]. *焊接学报*, 2016, 37(5): 69-72, 132.
- [11] Liu L M, Qi X D. Effects of copper addition on microstructure and strength of the hybrid laser-TIG welded joints between magnesium alloy and mild steel [J]. *Journal of Materials Science*, 2009, 44(21): 5725-5731.
- [12] Zhao L M, Zhang L L. Effect of Zn-xAl interlayer on microstructure and mechanical properties of Mg/steel joint [J]. *Journal of Dalian Jiaotong University*, 2017, 38(5): 79-84. 赵丽敏, 张琳琳. Zn-xAl 中间层对镁/钢接头组织和性能的影响 [J]. *大连交通大学学报*, 2017, 38(5): 79-84.
- [13] Zhai L L, Ban C Y, Zhang J W. Research status of mechanism of electromagnetic field in laser welding process [J]. *Hot Working Technology*, 2019, 48(15): 12-17, 21. 翟璐璐, 班春燕, 张峻巍. 激光焊接过程中电磁场作用机理的研究现状 [J]. *热加工工艺*, 2019, 48(15): 12-17, 21.
- [14] Avilov V, Fritzsche A, Bachmann M, et al. Full penetration laser beam welding of thick duplex steel plates with electromagnetic weld pool support [J]. *Journal of Laser Applications*, 2016, 28(2): 022420.
- [15] Liu H X, Cai C X, Jiang Y H, et al. Influence of alternative magnetic field on macro morphology and microstructure of laser cladding Fe-based composite coating [J]. *Optics and Precision Engineering*, 2012, 20(11): 2402-2410. 刘洪喜, 蔡川雄, 蒋业华, 等. 交变磁场对激光熔覆铁基复合涂层宏观形貌的影响及其微观组织演变 [J]. *光学精密工程*, 2012, 20(11): 2402-2410.
- [16] Ding H, Xu J L, Tan W S, et al. Influence of magnetic field on properties of Fe/Al dissimilar metal laser welding joints [J]. *Chinese Journal of Lasers*, 2017, 44(9): 0902003. 丁浩, 徐家乐, 谭文胜, 等. 磁场对激光焊接钢/铝异种金属焊缝性能的影响 [J]. *中国激光*, 2017, 44(9): 0902003.
- [17] Song G, Li T T, Zhang Z D, et al. Investigation of unequal thickness Mg/steel butt-welded plate by hybrid laser-tungsten inert gas welding with a Ni interlayer [J]. *Journal of Manufacturing Processes*, 2017, 30: 299-302.
- [18] Li T T. The research on the forming and interface strengthening mechanism of Mg alloy/steel by laser-induced arc fusion welding [D]. Dalian: Dalian University of Technology, 2020. 李涛涛. 镁合金/钢激光诱导电弧熔化焊成形及界面强化机制研究 [D]. 大连: 大连理工大学, 2020.

Microstructure and Properties of Laser Welding-Brazing Welded Joint of Mg/Steel with Ni Interlayer Assisted by Alternating Magnetic Field

Rong Yi, Cheng Donghai*, Xiong Zhenyu, Chen Yiping, Liu Zhaoze

School of Aeronautical Manufacturing Engineering, Nanchang Hangkong University, Nanchang, Jiangxi 330063, China

Abstract

Objective Universal demands to reduce energy consumption and emissions have elevated the role of lightweight design in the fields of aviation, ship, and automobile. These demands can be satisfied using Mg/steel dissimilar materials welding; however, many problems must be considered when attempting to realize a high-quality connection between Mg alloy and steel. The physical, chemical, and mechanical properties of Mg alloy and Fe are quite different. In addition, they are immiscible, and no intermetallic compounds are produced between Fe and Mg. Currently, to solve this problem, the formation of interfacial compounds is promoted by adding or coating an Ni, Cu, Ag, Zn, Sn, Cu-Zn, and Zn-xAl interlayer. Applying alternating magnetic field during laser welding process mainly brings two effects, including skin effect and electromagnetic force. When an alternating magnetic field is applied, liquid metal will produce an alternating induced current, which has a skin effect. In addition, the magnetic field and induced current produce an electromagnetic force; the alternating electromagnetic force promotes the positive and negative rotation of the molten pool, and convection in the molten pool is intensified. Previous studies have shown that the external alternating magnetic field can improve the weakness of joint compounds in the welding process of Mg/steel dissimilar materials. Ni can form intermetallic compounds and a solid solution with Mg and Fe, respectively. An alternating magnetic field is expected to regulate the distribution of compounds, which will improve the mechanical properties of joints. Therefore, laser welding-brazing technology assisted by alternating magnetic field is adapted to Mg/steel dissimilar materials welding with Ni interlayer. Microstructure and mechanical properties of the joint with and without alternating magnetic field are compared. The Mg/steel dissimilar metal connection with the Ni interlayer technology is further improved by applying an alternating magnetic field, and relevant data support is provided.

Methods Experimental materials included AZ31B Mg alloy and Q235 low carbon steel. The dimensions of Mg alloy and steel plates were 120 mm × 60 mm × 1 mm. A 0.1 mm thick pure Ni foil (99.9%) was used as the interlayer. The dimensions of the Ni foil were 60 mm × 10 mm × 0.1 mm. A 6 kW fiber laser (IPG YLS-6000CUT) was used for welding, and the laser beam was focused as a spot with a 0 mm diameter on the plates. During welding, the top surface of the plates was protected by argon with 99% purity at a flow of 15 L/min. AZ31B Mg alloy was lapped on Q235 low carbon steel with a clamp, and a 0.1 mm Ni foil was sandwiched between Mg alloy and the Q235 low carbon steel. After welding, the sample was cut along the direction perpendicular to the weld seam using a wire cutting machine, and the inlay was made using an XQ-1 hot mosaic machine and then polished. According to a preliminary test, the optimum welding parameters were $P = 1250$ W, $v = 20$ mm/s; the alternating magnetic field parameters were excitation current, $I_E = 0.8-2.0$ A (every 0.2 A is an increasing unit) and excitation frequency, $f = 15-55$ Hz (every 10 Hz is an increasing unit). Scanning electron microscope and energy dispersion spectrometer were used to study the cross-section morphology, Mg side weld zone, steel side weld zone, and intermetallic compound (IMC) layer of the joint under longitudinal alternating magnetic field. A WDW-100 electronic universal tensile testing machine was used to conduct tensile and shear tests on the joint. The tensile rate was 0.5 mm/min. Three groups of samples were stretched with each parameter. The average value of the three groups of parameters was calculated to determine the corresponding tensile and shear strength.

Results and Discussion The diffusion and reaction of Mg, Ni, and Fe elements in weld metal were promoted by strong electromagnetic stirring after applying the alternating magnetic field (Figs. 3 and 4). The appearance of zonal structures of Fe-Ni solid solution in the weld pool of Mg side weld zone and the serrated Mg₂Ni in the brazing zone of the IMC layer enhanced the mechanical bite effect. A continuous nanoscale AlNi layer was formed in the fusion welding zone, and this strengthened the joint (Figs. 5 and 6). With increased excitation current I_E and excitation frequency f , the tensile and shear strength σ_b of the joint initially increased and then decreased. For $P = 1250$ W, $v = 20$ mm/s, $I_E = 1.2$ A, and $f = 35$ Hz, the maximum σ_b of the joint reached 228 MPa, which was

approximately 15% higher than that without the magnetic field (Fig. 8).

Conclusions It is expected that the compound distribution of Mg/steel joints can be controlled by applying an alternating magnetic field, and the mechanical properties of the joints can be improved. The diffusion and reaction of Mg, Ni, and Fe elements in weld metal were promoted via strong electromagnetic stirring after applying the alternating magnetic field. The appearance of zonal structures of the Fe-Ni solid solution in the weld pool of the Mg side weld zone and the serrated Mg_2Ni in the brazing zone of the IMC layer enhanced the mechanical bite effect. A continuous nanoscale AlNi layer was formed in the fusion welding zone, and it strengthened the joint. With increased excitation current I_E and excitation frequency f , the tensile and shear strength σ_b of the joint increased initially and then decreased. For $P = 1250$ W, $v = 20$ mm/s, $I_E = 1.2$ A, and $f = 35$ Hz, the maximum σ_b of the joint reached 228 MPa, which is approximately 15% higher than that without the magnetic field.

Key words laser technique; laser welding-brazing technology; alternating magnetic field; mechanical bite; IMC layer; tensile and shear strength

OCIS codes 140.3390; 160.3900; 180.5810